Journal of Engineering and Applied Sciences 12 (20): 5147-5159, 2017
ISSN: 1816-949X

Variable Density Approach for Modeling of Transcritical and Supercritical Jets

Eduardo Antunes, Andre Silva and Jorge Barata
Department of Aerospace Sciences, Universidade da Beira Interior, Covilha, Portugal

Abstract: In order to study the high pressure and high temperature operating condition of a variety of internal combustion engines such as modern diesel engines, gas turbines and liquid fuel rocket engines, a cryogenic nitrogen jet injected into supercritical chamber conditions was simulated numerically. The favre averaged navier-stokes equations were employed together with a "k-ε" Turbulence Model and using instead of an ideal gas equation of state, the Amagat's law in an approach originally conceived for gaseous turbulent jets with variable density. The present study describes the assessment of the capabilities of the approach by comparison against experimental data as well as numerical simulation performed by other researcher. The obtained results show an acceptable agreement with experiments for the axial density distribution, failing slightly in the prediction of the jet potential core. Good agreement is observed for radial density distribution as well as for the jet spreading rate.

Key words: Critical point, cryogenic jets, fuel injection, rocket engines, supercritical flows, simulation

INTRODUCTION

The extremely important objective of prevention of further climate changes and exhaustion of natural resources in our planet demands the reduction of emissions and fossil fuel consumption of combustion engines. Also, in order to continue the progress in the understanding of our universe, better performance and reliability of rockets engines are required.

Increasing the operating pressure and temperature of combustion engines such as diesel engines, gas turbines, rocket engines and others is a known way of increasing efficiency and performance. Over the past years this increase has become an important trend in the design of new power units.

The process of fuel injection plays one of the most important roles in the subject of combustion. The way fuel and oxidizer mix inside the combustion chamber of the several kinds of engines is key for the degree of combustion efficiency in power production, additionally, the maximum performance possible to extract from a power system is strongly dependent on fuel injection. Combustion instability problems in rocket engines that affect reliability and can recurrently lead to destructive failures in such systems are often linked to the process of fuel injection (Sutton and Biblarz, 2010).

Thus, in recent combustion engines, the investigation of fuel (and oxidizer) injection into combustion chambers at high values of temperature and pressure has appeared as an important issue. However, it happens that when operating pressure and temperature increase, the fuels and oxidizers used by the propulsion systems may experience the exceeding of their critical values. The issue is that under conditions of pressure and temperature which are around or exceed the critical values, the behavior of the fluids is quite distinct than the one observed in conditions far from these (Bellan, 2000).

Several researcher have investigated jet in general and in particular the fluid behavior under and near supercritical conditions both by experimental and numerical approaches which resulted in the production of extensive bibliography (Antunes *et al*., 2011; Barata and Silva, 2003; Bellan, 2000; Chehroudi *et al*., 2002a, b; Mayer *et al*., 1998; Jarczyk and Pfitzner, 2012; Kim *et al*., 2011; Lacaze and Oefelein, 2012; Martinez *et al*., 2008; Mayer *et al*., 2003; Newman and Brzustowski, 1971; Oschwald, 2002; Oschwald and Schik, 1999; Oschwald *et al*., 2006; Papamoschou and Roshko, 1988; Park, 2012; Sanders *et al*., 1997; Schmitt *et al*., 2009, 2012; Seebald and Sojka, 2011; Segal and Polikhov, 2008; Shinjo and Umemura, 2011; Sierra *et al*., 2009, 2012; Zhou *et al*., 2011; Zong and Yang, 2006; Zong *et al*., 2004). As far as today, some conclusions have been reached and validated about the changes in the physical properties of fluids when they are around and above critical conditions. According to Bellan (2000) at the critical point mass diffusivity, surface tension and latent heat vanish. On the other hand, the heat capacity at constant pressure, Cp, the isentropic compressibility, k_s and the thermal conductivity, λ, all become infinite. At

Corresponding Author: Eduardo Antunes, Department of Aerospace Sciences, Universidade da Beira Interior, Covilha, Portugal

supercritical conditions which are characterized in the present research by assuming both pressure and temperature above their respective critical points, a behavioral change is observed for the jet structure which evolves from a liquid-gas injection to a gas-gas like injection (Chehroudi *et al*., 2002; Oschwald, 2002; Oschwald *et al*., 2006; Segal and Polikhov, 2008). However, bigger questions appear about fluid behavior in conditions near critical for which it is still unknown if the fluid presents a behavior closer to a gas, a liquid or a mix of the two. Recent studies have pointed in the direction of identifying four different regions around the critical point. These regions are dependent on whether both pressure and temperature are supercritical, just one of them or none. The the rmodynamic region of the flow will strongly determine its behavior (Lacaze and Oefelein 2012).

Past researcher, Antunes *et al*. (2012), Barata and 2003) attempted to evaluate the applicability of a numerical variable density approach to cryogenic nitrogen jets injected into nitrogen gaseous environment for different chamber-to-injectant density ratio (ω). The results obtained were focused on the prediction of the jet spreading rate based on the half width of half maximum of density. Was attempted to establish a limit of applicability of the approach in terms of ω. And was shown agreement with the experimental work of Chehroudi for chamber-to-injectant ratios between 0.025 and 0.1408.

The aim of the presentis research to study, evaluate and develop numerical methods which are suitable to more accurately describe the injection process in its various parameters, around and beyond critical condition. The present study describes the injection of liquid nitrogen into gaseous nitrogen environment, consisting of a continuation and development of a previous work from the same Antunes with the imposition of different boundary conditions as well as a different mesh. A favre averaged navier-stokes approach is adopted using a "k-ε" Turbulence Model initially developed for incompressible but variable density flows. Two different test cases were simulated using the same injector and chamber geometry shown in Fig. 1. A transcritical and a supercritical case were simulated and their conditions are shown in Table 1. The transcritical case (supercritical pressure but subcritical temperature) corresponds to the case number 3 by Mayer *et al*. (2003) and the supercritical simulation to the case 4 of the same researcher. The only difference between the transcritical case and the supercritical case is the injection temperature that is higher in the second case, however, this difference is enough to place them in two different the rmodynamic regimes. The modeled cases were then compared with the experimental data by Mayer *et al*. (2003) and the large eddy simulations by

Table 1: Conditions of the test cases

Conditions	Case 3 transcritical	Case 4 supercritical
Chamber temperature (K)	298	298
Chamber pressure (MPa)	3.97	3.97
Injection temperature (K)	126.9	137
Injection velocity (m/sec)	4.9	5.4
ρ_0 (kg/m^3)	435	171
ρ_∞ (kg/m^3)	45.5	45.5
ω	0.1046	0.2661

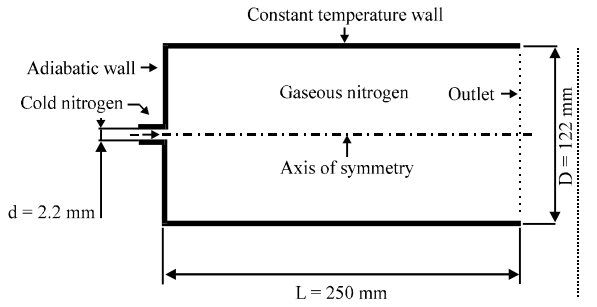

Fig. 1: Chamber geometry

Schmitt *et al*. (2009), Jarczyk and Pfitzner (2012). These two tests in combination with the knowledge obtained in previous researcher are expected to give a better insight into the injection phenomenon performed at conditions close to critical. Such an analysis is crucial to obtain more clues about whether the strategies adopted to model these flows are accurate enough.

MATERIALS AND METHODS

For the current investigation, the mathematical model and numerical approach followed the same line already used by Barata and Silva (2003) and in previous (Antunes *et al*., 2011). This method is described in great detail by Sanders *et al*. (1997). In Sanders's publication is described a second order model for which differential equations are used for the calculation of reynolds stresses and a first-order (k-ε) Model. In the current work only the first order model was employed.

Governing equations: The method originally developed to solve variable density jet flows is based on the solution of the conservation equations for momentum and mass. Turbulence is modeled with the "k-ε" Turbulence Model. A similar method has been used for three-dimensional or axisymmetric flows (Antunes *et al*., 2011; Barata and Silva, 2003; Sanders *et al*., 1997) and only the main features are summarized here.

In the conservation equations, mass weighted averaging is applied to avoid the appearance of many terms involving density fluctuations for which additional models are needed. A favre averaged or mass weighted averaged, quantity is defined as:

$$\tilde{\phi} = \frac{\overline{\rho\phi}}{\overline{\rho}} \quad (1)$$

For the governing equations, the standard parabolic truncation is employed. The mass averaged partial differential equations governing the steady, variable density axisymmetric flow may be written in cylindrical polar coordinates as:

$$\frac{\partial \overline{\rho}UU}{\partial x} + \frac{1}{r}\frac{\partial r\overline{\rho}UV}{\partial r} = -\frac{\partial \overline{\rho}}{\partial x} - \frac{1}{r}\frac{\partial r\overline{\rho}\overline{u'v'}}{\partial r} \quad (2)$$

$$\frac{\partial \overline{\rho}UV}{\partial x} + \frac{1}{r}\frac{\partial r\overline{\rho}VV}{\partial r} = -\frac{\partial \overline{\rho}}{\partial x} - \frac{1}{r}\frac{\partial r\overline{\rho}\overline{v'v'}}{\partial r} + \overline{\rho}\frac{\overline{w'w'}}{r} \quad (3)$$

and the continuity equation as:

$$\frac{\partial \overline{\rho}U}{\partial x} + \frac{1}{r}\frac{\partial r\overline{\rho}V}{\partial r} = 0 \quad (4)$$

To describe the mixing of gases, the mixture fraction F that represents the mass fraction of the nozzle fluid is introduced. It obeys a convection-diffusion equation of the form:

$$\frac{\partial \overline{\rho}UF}{\partial x} + \frac{1}{r}\frac{\partial r\overline{\rho}VF}{\partial r} = -\frac{1}{r}\frac{\partial r\overline{\rho}\overline{v'f}}{\partial r} \quad (5)$$

In "k-ε" Turbulence Model, the Reynolds stresses are expressed in terms of the local strain rate:

$$-\overline{\rho}\overline{u'_i u'_j} = \overline{\rho}(\nu_t + \nu)\left(\frac{\partial \tilde{u}_i}{\partial x_j} + \frac{\partial \tilde{u}_j}{\partial x_i}\right) - \frac{2}{3}\delta_{ij}\left(\overline{\rho}k + \overline{\rho}(\nu_t + \nu)\frac{\partial \tilde{u}_j}{\partial x_j}\right) \quad (6)$$

With:

$$\nu_t = C_\mu \frac{k^2}{\varepsilon} \quad (7)$$

The scalar flux in Eq. 5 is approximated with a gradient transport assumption:

$$\overline{u'_i f'} = -\frac{\nu_t}{\sigma_f}\frac{\partial F}{\partial x_i} \quad (8)$$

From the foregoing, we can deduce the parabolized set of equations in cylindrical coordinates where the generalized equation is:

$$\frac{\partial}{\partial x}\left(\overline{\rho}U\tilde{\phi}\right) + \frac{1}{r}\frac{\partial}{\partial r}\left(r\overline{\rho}\tilde{\phi}\right) = \frac{1}{r}\frac{\partial}{\partial r}\left(r\overline{\rho}D\frac{\partial \tilde{\phi}}{dr}\right) + S_\varphi \quad (9)$$

Where:

$\tilde{\phi}$ = May stand for any of the velocities, turbulent kinetic energy, dissipation or scalar property

S_ϕ = Take on different values for each particular $\tilde{\phi}$ as described in detail by Sanders *et al.* (1997)

To obtain the mean density an equation of state based on the Amagat's law is employed using the mean mixture fraction. With constant pressure this leads to:

$$\frac{1}{\overline{\rho}} = \frac{F}{\rho_o} + \frac{1-F}{\rho_\infty} \quad (10)$$

where, density fluctuations have been neglected. This is allowed in isothermal jets because the instantaneous density for which Eq. 10 is exact is approximately a linear function of the instantaneous mixture fraction (Barata and Silva, 2003).

Numerical method: The governing equations are solved using a parabolized marching algorithm similar to the one reported in the (elliptic) TEACH code (Sanders *et al.*, 1997). The computations are performed by using the continuity equation to obtain the radial Velocity (V). In fact, it has been found Sanders *et al.* (1997) that using the radial momentum equation for V and solving a pressure correction equation for V in radial direction did not result in any difference when compared with the use of the continuity equation. In this approach, the numerical model was applied to variable density jets and for the present case it was used for the study of liquid cryogenic jets under sub-near critical pressures and sub to supercritical temperatures.

In order to determine the tangent of the jet spreading angle, the Half Width of Half Maximum of the density (HWHM of density) is used.

Computational grid: The flow configuration can be observed in Fig. 1 with the cold nitrogen being injected through a round injector with 2.2 mm of diameter into a cylindrical chamber with a diameter of 122 mm and a length of 250 mm. The boundary conditions are well described in the same Fig. 1 with the imposition of a constant temperature wall in the north boundary, an adiabatic wall at the west boundary and the outlet condition exists in the east boundary. For this numerical approach and since the flow is axisymmetric, it was only modeled half of the domain seen in Fig. 1 and thus the south boundary is the symmetry axis. Therefore, the

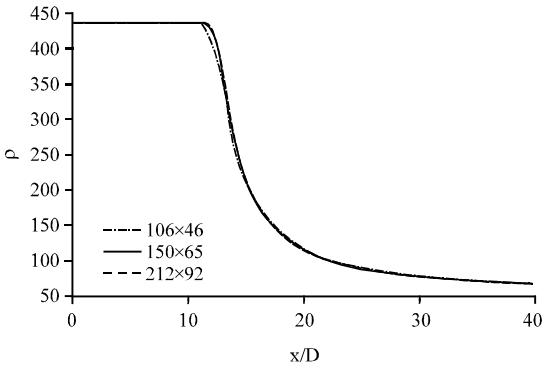

Fig. 2: Grid size dependency test based on the axial density distribution

numerical domain becomes 250 mm long and 61 mm width. A grid was used with 150 points in the axial direction and 65 points in the radial direction making a total of 9150 points.

In the construction of the grid, care was taken in order to assure that the defined computational domain was always kept independently of the size of the grid. Also, a higher refinement was introduced close to the injector where higher variable gradients are expected and biggest interest exists for the current investigation. The grid follows a constant expansion in the axial direction with the initial length size of the control volume being defined by the expansion rate and number of points imposed. For the radial direction, the initial distance between knots is kept contact during all the injector width and then follows a constant expansion until reaching the north boundary.

Because a new grid was used and no other previous works had used it before, a grid dependency test was performed. The axial density distribution was used to test the grid dependency of the computations. Figure 2 compares the evolution of the density distribution along the symmetry axis for 3 different grid sizes. With a grid size of 106×46 points, approximately half of the size in number of points, the results are already very close from those obtained from the used grid (150×65). And for the grid with approximately twice the size in number of points (212×92) the difference is negligible. It can be concluded that for the used grid size the results do not depend on the grid size.

RESULTS AND DISCUSSION

The numerical results obtained in the present research are presented in this section. To assess the accuracy of the simulations performed, the results are compared against the experimental data by Mayer *et al.* (2003) and large eddy simulations carried out by Schmitt *et al.* (2009), Jarczyk and Pfitzner (2012). A discussion is also provided in order to reach the conclusions exposed in the next section.

Figure 3-5 shows the velocity, mixture fraction and density fields, respectively for transcritical and supercritical cases. Its allow us to obtain a general picture of the flow geometry. As said before and highlighted in Table 1, the two test cases only differ from each other in the injection temperature (and consequently the injection density) and velocity while the chamber conditions remain the same for both cases. Nevertheless, this difference in the injection temperature between the two cases is enough to position them in different thermodynamic regimes. In the transcritical case, the pressure in supercritical while the temperature is subcritical while for the supercritical case both pressure and temperature are supercritical.

Comparison between both cases shows very similar jet structures. Nevertheless, the supercritical case presents a faster reduction of the density and mixture fraction value than the transcritical case. Similar conclusions are obtained in the previous studies of Schmitt *et al.* (2009), Jarczyk and Pfitzner (2012) with the LES visualizations showing similar variations between the two cases. These results also suggest the existence of a smaller potential core for the supercritical conditions shown in case 4. This characteristic, in particular will be discussed later.

Figure 3 shows the velocity fields obtained in each of the simulations performed. It is visible in both cases the appearance of an entrainment close to the injector exit with ambient nitrogen being pulled into the jet stream. This phenomenon appears to be slightly more intense in transcritical regime even having a slower injection velocity. This is probably due to the higher jet momentum caused by higher injection fluid density. It is also visible that farther away from the injector, the velocity vectors are bigger in the transcritical case than in the supercritical due not only to the higher injection velocity but by the higher fluid density. The injection density appears to be determinant to the distance that a jet can reach.

In Fig. 4, the mixture fraction fields are shown for test both tested cases. The images show a high concentration of injected fluid close to the injector exit which decreases as the distance to the injector in both radial and axial direction increases. Comparison between the two cases shows a faster decrease of the mixture fraction along the jet in supercritical conditions than in transcritical. However, it is important to note that this faster decrease does not mean an enhanced mixture of the jet fluid with the chamber fluid. In fact there are higher mixture fraction gradients at supercritical

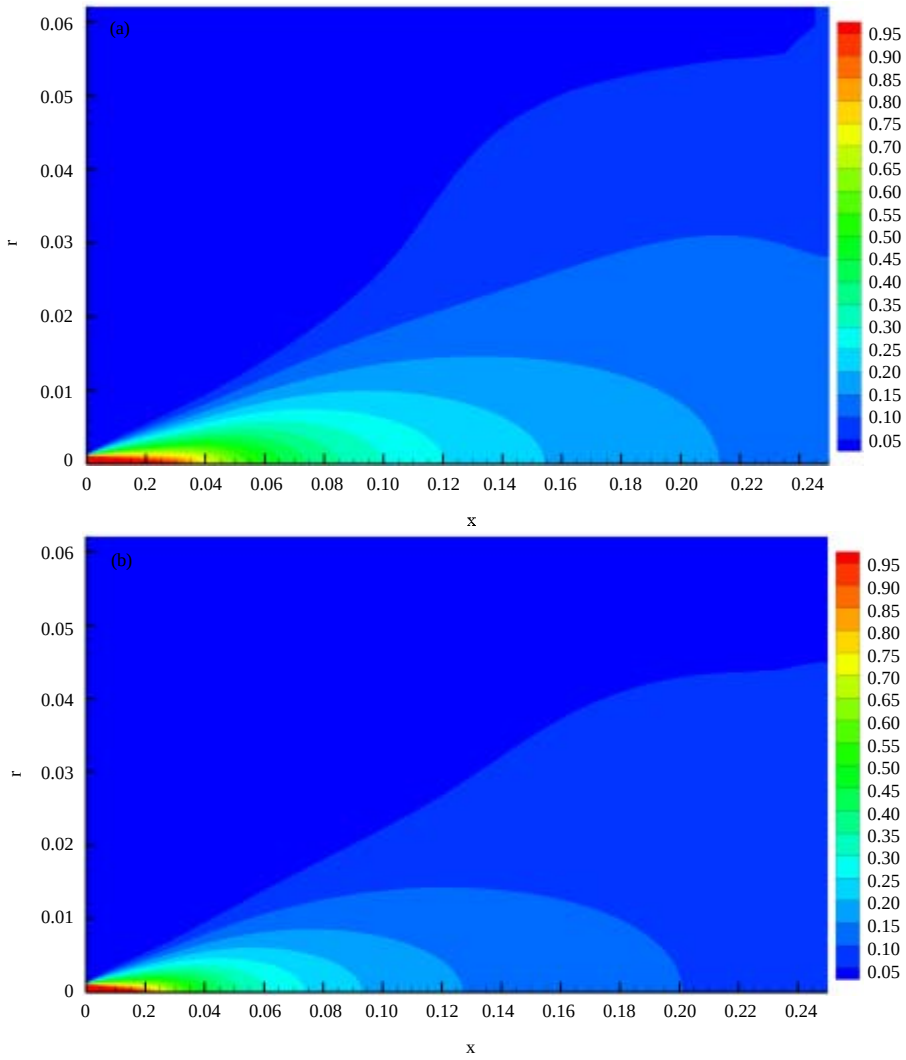

Fig. 3: Velocity field of the jet for: a) transcritical and b) supercritical conditions

conditions. Close to the injector the mixture fraction quickly decreases in value but then in the rest of the injection chamber, the domain is dominated by mixture fraction values bellow 0.5. In the transcritical case, even though it evidences a slower decrease of mixture fraction and bigger penetration of injection fluid (apparently showing a slower mixture at the beginning of the jet) an increased mixture is still visible as the mixture fraction values close to 0.5 are found in most of the domain. These results of the apparently increased mixture in the case with smaller temperature and at which the difference between injection density and chamber density is higher can be considered in some way surprising.

The density fields are shown in Fig. 5. Again the results show similar jet structure for both cases. The transcritical case, however, shows a longer dense core than the one observed at supercritical conditions. Having the transcritical situation a higher density gradient between injected and chamber fluid and a lower injection velocity, one could expect it to have a shorter dense core as well as a smaller jet penetration than supercritical casa. However, the opposite occurs. The explanation found by the researchers of the present study is that the fluid density due to its influence in fluid momentum, rules the jet dynamics. Although, the jet in transcritical conditions has a slower injection velocity, it has in fact, a higher momentum which results in a bigger penetration length.

The higher jet momentum is also responsible for the more intense entrainment at the jet exit in this case. The entrainment phenomenon is important for the fluid mixing. This explains the enhanced mixing at transcritical conditions when compared to supercritical. These results obtained by the present numerical approach are

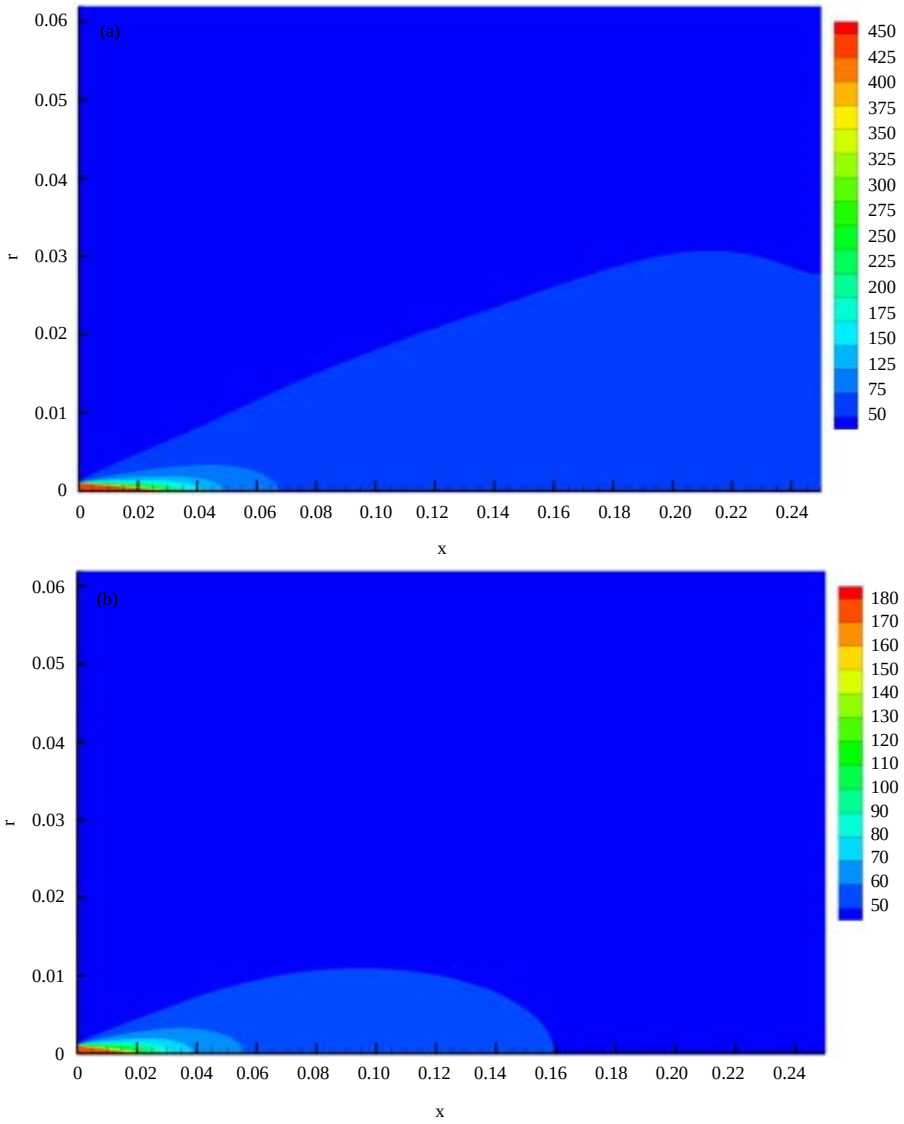

Fig. 4: Mixture fraction field of the jet for: a) transcritical and b) supercritical conditions

corroborated in the LES results by Schmitt *et al.* (2009) where case 3 also shows a longer jet length and a denser core than case 4.

The results obtained by the velocity and scalar fields also give us the evidence that the jet behavior is mostly dominated by the convection terms while diffusion plays a minor role. In turn, convection is mostly dominated by the density. The calculation of density appears this way as a key factor in the modeling of this kind of flows.

The axial density distributions of transcritical and supercritical cases are shown in Fig. 6 and 7, respectively. The present numerical model is evaluated against experimental and numerical results of other researcher. Potential core length is one important characteristic of a jet, generally used by other researchers to help to quantify it. Schmitt *et al.* (2009) defines the potential core length as the axial distance at which the centerline density is 99% of the injected density. Generally, potential core length is expressed in multiples of injector diameters. In the present investigation, it was decided to use the same definition of potential core already used by Schmitt *et al.* (2009).

The results obtained for the transcritical case in the present investigation show a potential core of 11.8 injector diameters. It is longer when compared with the results of other researchers. Schmitt *et al.* (2009) for example shows a potential core length of 7.9 diameters, where as Jarczyk and Pfitzner (2012) identifies a length of around 9 diameters. The large eddy simulation performed by Schmitt *et al.* (2009) shows the best agreement with the

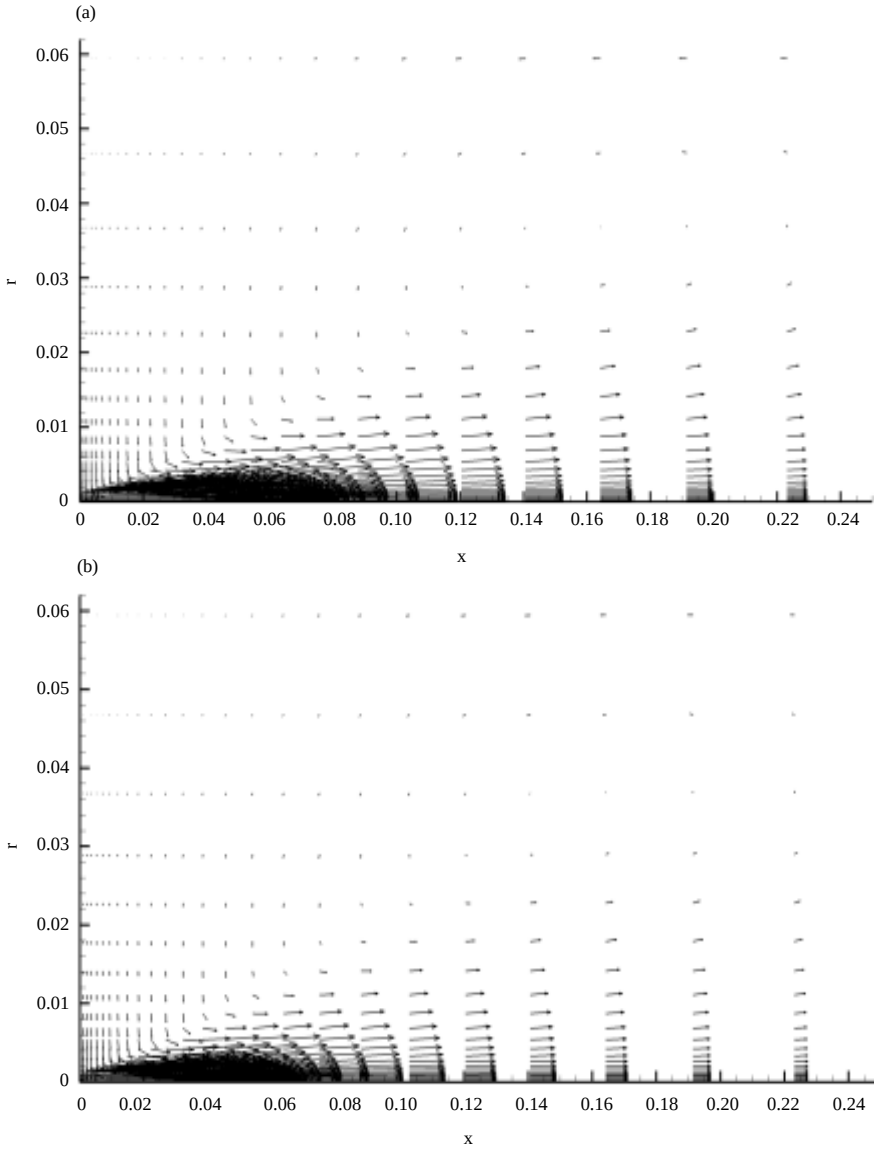

Fig. 5: Density field of the jet for: a) transcritical and b) suppercritical conditions

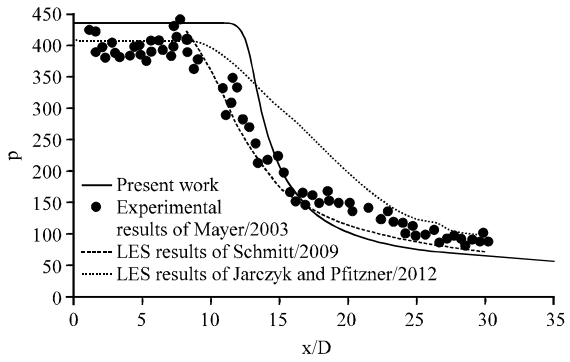

Fig. 6: Axial density distribution for transcritical case and comparisons with different researcher's results

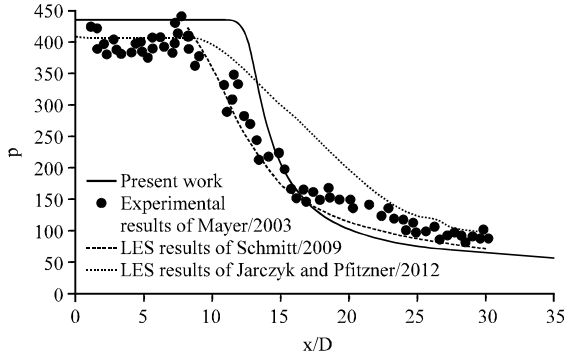

Fig. 7: Axial density distribution for supercritical case and comparisons with different researcher's results

experimental data from all the numerical approaches. The large eddy simulation by Jarczyk and Pfitzner (2012) overestimates the value of the density for a large range of the visible domain from the potential core and only getting closer to the experimental values at an axial distance of around 25 jet diameters. The current approach after clearly overestimating the potential core gets closer to the experimental data for a distance of 15×/D, however, diverges from the experiments after 17×/D. The results are nevertheless in line with the other investigations. The same kind of centerline density distribution profile was obtained for supercritical conditions in Fig. 7. The potential core obtained of around 7.8 diameters is bigger than the one obtained with the two LES results which are 5.1 diameters in the work by Schmitt *et al.* (2009) and around 6 jet diameters for Jarczyk and Pfitzner (2012). Analyzing experimental data by Mayer *et al.* (2003), there is little amount of evidence of the existence of a potential core for this test case. For the supercritical test case, the numerical approach published by Jarczyk and Pfitzner (2012) provides the results with the closest agreement with the experimental data. The numerical results by Schmitt *et al.* (2009) under predict the density value at the centerline for all the visible domain with the exception of the points closest to the injector. The results of the present approach after the overestimation of the potential core under predict slightly the density value, gives, however, closer results to experimental data than Schmitt *et al.* (2009). Further, away from the injector the current results reach total agreement with the data from Schmitt.

Figure 8 and 9 show the radial density distribution of three different axial distances for transcritical and supercritical cases, respectively. Figure 8a-c illustrate

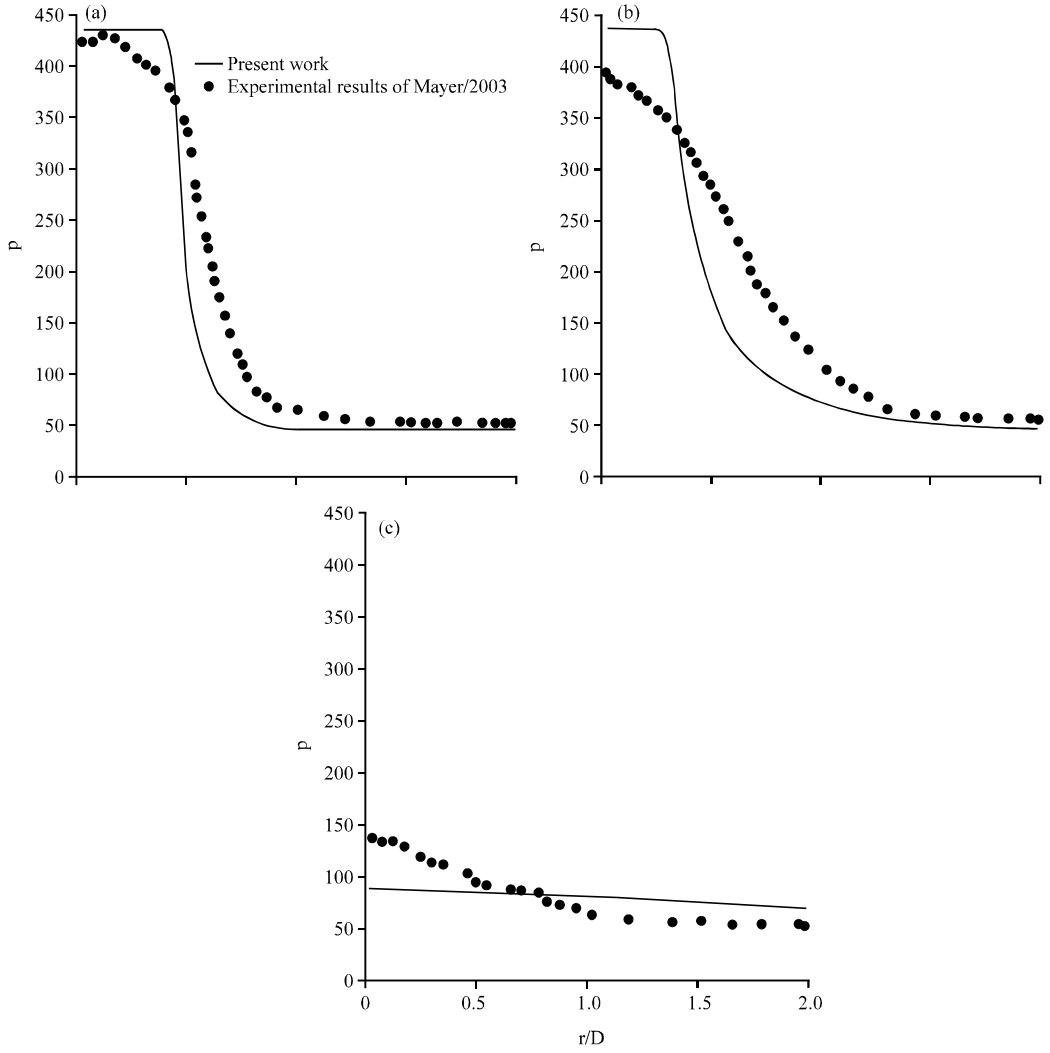

Fig. 8: Radial density distribution for transcritical case: a) x/D = 1.2; b) x/D = 5 and c) x/D = 25

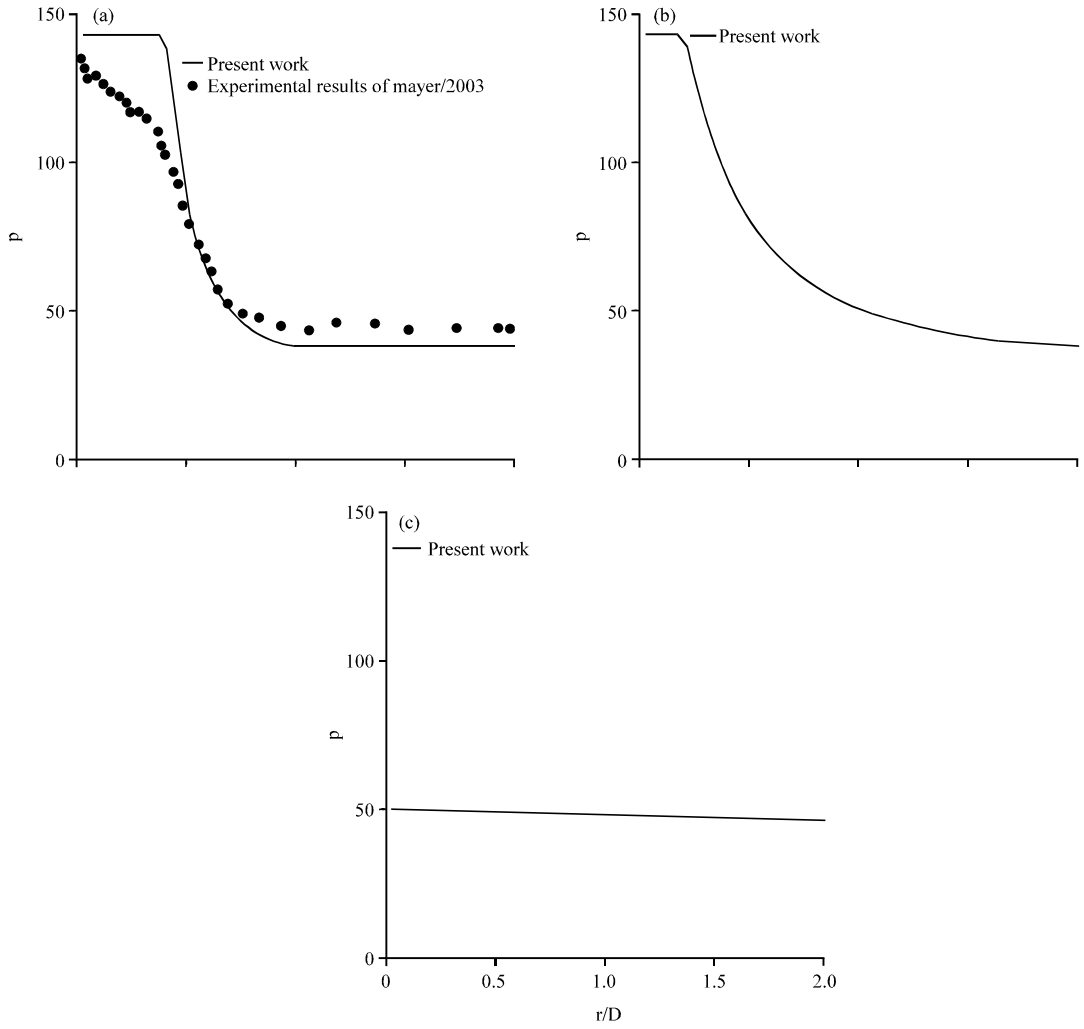

Fig. 9: Radial density distribution for supercritical case: a) x/D = 1.2; b) x/D = 5 and c) x/D = 25

the axial distance of 1.2, 5 and 25 injector diameters, respectively. Figure 8a shows quite good agreement with experimental data by Mayer *et al*. (2003). For the same axial distance for supercritical conditions in Fig. 9a, the agreement is also good showing even an interception of experimental and numerical data during some range of the domain. For the axial distance of 5 x/D in case 3, Fig. 8b, the experimental data show a decrease of density close to the centerline that is not observed in the current results. These results are naturally attributed to the longer potential core, obtained in the current approach which have already been visualized in Fig. 6. Farther away from the centerline the numerical results find much closer agreement with the experiments. For the same case in Fig. 8c at an axial distance of 25 x/D, the agreement obtained is not as good, since the numerical results are not able to replicate the flattened bell shape of the experimental data which shows an almost constant value of density along the radial direction with only a slight decrease. For supercritical case, it can be observed that the results follow the same trend of case 3 and a similar agreement is expected. The comparison between present results and experimental data shows a fair agreement between both with some differences identified further downstream in the domain, showing some difficulty of the current approach to provide correct values of density in this zone. The spreading angle of the jet is one of the most important parameters available to the use of a researcher when his objective is to characterize a jet. In order to determine the spreading of a jet, it becomes necessary to define the radial border of it. Several researchers including those cited in the present study by Jarczyk and Pfitzner (2012), Schmitt *et al*. (2009) assume that the border of the jet is in the radial position where the

Table 2: Results of jets spreading rate

Variables	Oschwald (2002)	Mayer *et al.* (2003)	Schmitt *et al.* (2009)	Present work
Transcritical case	0.206	0.196	0.227	0.316
Supercritical case	0.312	-	0.241	0.310

density is the average between the maximum value (located in the centerline position at the same axial distance) and minimum value (the chamber density). This is how the Full Width of Half Maximum of density (FWHM of density) is defined. In the research by Schmitt *et al.* (2009) the tangent of the spreading angle of density was obtained by linear interpolation of the FWHM of density between x/D = 15 and x/D = 25. In the present work, it was decided to use the exact same method.

Figure 10 shows the FWHM of density for test case at transcritical conditions obtained in the present research and is compared against the Raman measurements by Mayer *et al.* (2003). It can be observed that the numerical results obtained in the present work follow a similar trend as the one obtained in the experimental data. The chart initially shows a decrease of the half width that extends up to 10×/D in the experimental data whereas in the present numerical data it decreases until approximately 12×/D but always with a smaller width than in the experimental data. After this point, the half width of the jet starts increasing, showing that the jet is spreading. The observed numerical spreading rate is very much in line with the Raman measurements. The values of the tangent of spreading angle using the FWHM of density are expressed in Table 2 for the experimental data by Oschwald (2002) and Mayer *et al.* (2003) the large eddy simulation by Schmitt *et al.* (2009) and the present research. At transcritical conditions a jet spreading rate tagent of around 0.2 is obtained by the two experimental works. The large eddy simulation by Schmitt *et al.* (2009) provides a slightly large value of spreading rate but still closer the value obtained by the present approach.

Figure 11 shows the FWHM of density for the supercritical case. For this case there were no available experimental data from the raman measurements by Mayer *et al.* (2003) and for this reason Fig. 11 only shows the results obtained in the present research. In the chart, it is possible to observe at the beginning of the jet a very slow decrease of the jet width until an axial length of around 8x/D. After this mark, there is an increase of the jet width following a tangent of the spreading angle of around 0.310. The results provided in Table 2 shows that for this case the present approach provides a spreading rate in very close agreement with the experimental data by Oschwald (2002) clearly outperforming the results obtained by Schmitt *et al.* (2009) with their large eddy simulation which under predict the value of the tangent of the spreading rate.

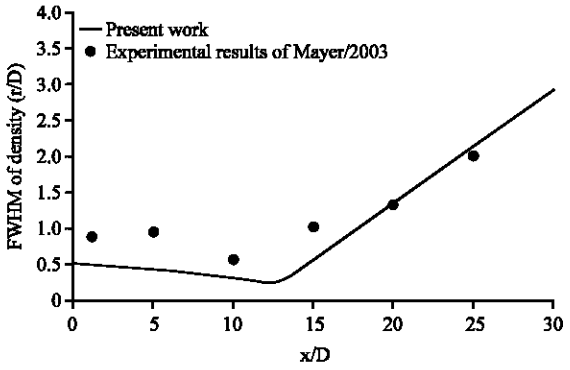

Fig. 10: Half width of half maximum of density for transcritical case and comparison with experimental data by Mayer *et al.* (2003)

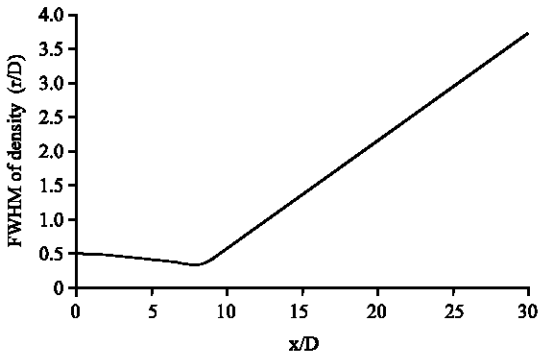

Fig. 11: Half width of half maximum of density for supercritical case

CONCLUSION

Aiming to study, evaluate and develop numerical methods for more accurately describing the injection process around and beyond critical conditions, a numerical approach-originally designed to model gaseous jet flows with different densities and used in previous works to study the jet spreading angle for different density ratios-has been evaluated to model cryogenic jets at thermodynamic conditions near critical. As part of the task is also the goal of attempting to identify and later integrate the needed modifications to the numerical approach in order to make it more suitable to simulate the flows of interest.

To validate the present numerical approach, the results were compared against the experimental data reported by Mayer *et al.* (2003) as well as two

computational results performed under LES techniques (Schmitt *et al*., 2009; Jarczyk and Pfitzner 2012) for two test cases. For the axial density distribution, the numerical results obtained in the present investigation show acceptable agreement with experimental results by Mayer *et al*. (2003) with comparable results to those obtained by the LES investigations (Jarczyk and Pfitzner, 2012; Schmitt *et al*., 2009). However, difficulties still arise in the calculation of a correct length of the potential core. Fairly good agreement was found for the radial density distribution with the results corroborating much of what was concluded in the axial density distribution. Close agreement with experimental data is achieved for the jet spreading rate. For the transcritical case the results are very comparable with experimental and not very far from the results provided by the large eddy simulation approach by Schmitt *et al*. (2009) which is a much more computationally expensive approach. For the supercritical case the present approach provides the closest agreement with the experimental data by Oschwald (2002) the large eddy simulation by Schmitt *et al*. (2009) isn't table to reach a similar level of agreement at a much higher computational cost.

There has been a trend, between researcher investigating jet at conditions near critical to use a real gas equation of state to calculate the density (Jarczyk and Pfitzner, 2012; Oschwald, 2002; Park, 2012; Schmitt *et al*., 2009). In the present numerical approach, the mean density is calculated by an equation of state that is a linear function of the mixture fraction. As stated above this method of calculation of density is allowed in isothermal jets. However, in the present test cases, one is not in the presence of isothermal gases so this method of calculating density can be one of the main causes of the discrepancies that still exist in density determination for instance in the calculation of potential core length. The use of this simplified method of calculating density is justified in the present approach by the objective of evaluating the potential of this method before departing to different techniques more suitable of producing more accurate results.

Transcritical and supercritical jets are known to be highly transient and very sensitive to small and local changes of temperature and pressure (Bellan, 2000). Reynolds or favre averaged navier-stokes methods, unlike LES, only use the average terms of velocity, pressure, temperature, etc. These approaches lead to the neglecting of the small fluctuations in transcritical and supercritical jets which can have a huge impact on the flow behavior. This reality could in fact also be one of the causes for incapacity of the present numerical approach to provide accurate predictions of the studied jet spreading angle. However, Park (2012) in his LES and RANS investigation, concluded that the suitable adoption of an equation of state is more decisive than the selection of turbulence model for the numerical performance. According to park, the potential core length is linked with the existing pseudo-boiling region. The pseudo-boiling region can be defined as the prolongation of the gas/liquid phase-change line and corresponds to a maximum of constant-pressure heat capacity at constant pressure (Petit *et al*., 2013). Thus in order to ba able to provide a correct prediction of the jet potential core one must be able to correctly predict the fluid properties at the transition between transcritical and supercritical conditions.

RECOMMENDATIONS

Future investigations will be focused on the integration of a real gas equation of state into the present numerical formulation providing to the model a different method for density calculation. With these changes, the researchers expect to improve the agreement with experiments for the transcritical injection case while keeping the same level of agreement already achieved for the supercritical outperforming more expensive large eddy simulations.

ACKNOWLEDGEMENTS

Researchers would like to thanks: Fundacao para a Ciencia e a Tecnologia (FCT) the Portuguese Public Agency for Science and Technology for the financing of the present investigation by providing a PhD scholarship to the first researchers with the reference SFRH/BD/87822/2012. Also, AeroG-LAETA associated laboratory for providing integration in a research unit to the researchers. And finally to Universidade da Beira Interior-Covilha, the host institution for the researchers.

NOMENCLATURE

C_μ = Coefficient in turbulence model
D = Injector Diameter (m)
ε = Dissipation rate of turbulent energy
f = Mixture fraction
F = Mean mixture fraction
i = Axial direction index
j = Radial direction index
k = Turbulent kinetic energy
ϕ = Generalized variable
ω = Chamber-to-injection fluid density ratio (p_∞/p_0)
P_{cr} = Critical Pressure (MPa)
P_∞ = Chamber ambient Pressure (MPa)
P_r = Reduced Pressure (P_∞/P_{cr})
ρ = Density ($kg.m^{-3}$)
ρ_0 = Injected fluid density ($kg.m^{-3}$)
ρ_∞ = Injection chamber's fluid density ($kg.m^{-3}$)
r = Radial coordinate (m)
R/D = Radial Distance normalized by injector diameter
R_{diam} = Injector radius (m)
R_e = Reynolds number

S_ϕ = Source term
t = Time (s)
T = Temperature (K)
u = Axial velocity ($m.s^{-1}$)
U = Mean axial velocity ($m.s^{-1}$)
U_{in} = Injection axial velocity ($m.s^{-1}$)
v = Radial velocity ($m.s^{-1}$)
v_t = Turbulent kinematic viscosity
V = Mean radial velocity ($m.s^{-1}$)
X = Axial coordinate (m)
x/D = Axial Distance normalized by injector diameter

REFERENCES

Antunes, E., A. Silva and J. Barata, 2011. Evaluation of numerical variable density approach to cryogenic jets. Proceedings of the 50th AIAA Meeting on Aerospace Sciences including the New Horizons Forum and Aerospace Exposition, January 9-12, 2012, A.I.A.A., Nashville, Tennessee, pp: 1-14.

Barata, M.J.M. and R.A.R. Silva, 2003. Numerical study of cryogenic jets under supercritical conditions. J. Propul. Power, 19: 142-147.

Bellan, J., 2000. Supercritical (and subcritical) fluid behavior and modeling: Drops, streams, shear and mixing layers, jets and sprays. Prog. Energy combust. Sci., 26: 329-366.

Chehroudi, B., R. Cohn and D. Talley, 2002a. Cryogenic shear layers: Experiments and phenomenological modeling of the initial growth rate under subcritical and supercritical conditions. Intl. J. Heat Fluid Flow, 23: 554-563.

Chehroudi, B., D. Talley and E. Coy, 2002b. Visual characteristics and initial growth rates of round cryogenic jets at subcritical and supercritical pressures. Phys. Fluids, 14: 850-861.

Jarczyk, M.M. and M. Pfitzner, 2012. Large eddy simulation of supercritical nitrogen jets. Proceedings of the 50th AIAA Meeting on Aerospace Sciences including the New Horizons Forum and Aerospace Exposition, January 9-12, 2012, A.I.A.A., Nashville, Tennessee, pp: 1-13.

Kim, T., Y. Kim and S.K. Kim, 2011. Numerical study of cryogenic liquid nitrogen jets at supercritical pressures. J. Supercrit. Fluids, 56: 152-163.

Lacaze, G. and J.C. Oefelein, 2012. A non-premixed combustion model based on flame structure analysis at supercritical pressures. Combust. Flame, 159: 2087-2103.

Martinez, M.S., F.A.C. Sanchez, J.M.R. Avila, A.G. Munoz and S.M. Aceves, 2008. Liquid penetration length in direct diesel fuel injection. Appl. Therm. Eng., 28: 1756-1762.

Mayer, W., J. Telaar, R. Branam, G. Schneider and J. Hussong, 2003. Raman measurements of cryogenic injection at supercritical pressure. Heat Mass Transfer, 39: 709-719.

Mayer, W.O.H., A. Schik, A.H. Vielle, C.B. Chauveau and K.I.G. Ograve *et al*., 1998. Atomization and breakup of cryogenic propellants under high-pressure subcritical and supercritical conditions. J. Propul. Power, 14: 835-842.

Newman, J.A. and T.A. Brzustowski, 1971. Behavior of a liquid jet near the thermodynamic critical region. AIAA. J., 9: 1595-1602.

Oschwald, M. and A. Schik, 1999. Supercritical nitrogen free jet investigated by spontaneous Raman scattering. Exp. Fluids, 27: 497-506.

Oschwald, M., 2002. Spreading angle and centerline variation of density of supercritical nitrogen jets. Atomization Sprays, 12: 91-106.

Oschwald, M., J.J. Smith, R. Branam, J. Hussong and A. Schik *et al*., 2006. Injection of fluids into supercritical environments. Combust. Sci. Technol., 178: 49-100.

Papamoschou, D. and A. Roshko, 1988. The compressible turbulent shear layer: An experimental study. J. Fluid Mech., 197: 453-477.

Park, T.S., 2012. LES and RANS simulations of cryogenic liquid nitrogen jets. J. Supercrit. Fluids, 72: 232-247.

Petit, X., G. Ribert, G. Lartigue and P. Domingo, 2013. Large-eddy simulation of supercritical fluid injection. J. Supercrit. Fluids, 84: 61-73.

Sanders, J.P.H., B. Sarh and I. Gokalp, 1997. Variable density effects in axisymmetric isothermal turbulent jets: A comparison between a first-and a second-order turbulence model. Intl. J. Heat Mass Transfer, 40: 823-842.

Schmitt, T., J. Rodriguez, I.A. Leyva and S. Candel, 2012. Experiments and numerical simulation of mixing under supercritical conditions. Phys. Fluids, Vol. 24,

Schmitt, T., L. Selle, B. Cuenot and T. Poinsot, 2009. Large-eddy simulation of transcritical flows. C.R. Mec., 337: 528-538.

Seebald, P. and P.E. Sojka, 2011. Supercritical and Transcritical Injection. In: Handbook of Atomization and Sprays, Nasser, A. (Ed.). Springer, New York, USA., ISBN:978-1-4419-7263-7, pp: 255-261.

Segal, C. and S.A. Polikhov, 2008. Subcritical to supercritical mixing. Phys. Fluids, 20: 1-7.

Shinjo, J. and A. Umemura, 2011. Surface instability and primary atomization characteristics of straight liquid jet sprays. Intl. J. Multiphase Flow, 37: 1294-1304.

Sierra, P.J., C.P. Santiago and F. Castro, 2012. Numerical modelling of supercritical submerged water jets in a subcritical co-flow. J. Supercrit. Fluids, 65: 45-53.

Sierra, P.J., S.M.T. Parra, S.J. Garcia, F. Castro and M.J. Cocero, 2009. Numerical analysis of high-pressure fluid jets: Application to RTD prediction in supercritical reactors. J. Supercrit. Fluids, 49: 249-255.

Sutton, G.P. and O. Biblarz, 2010. Rocket Propulsion Elements. 8th Edn., John Wiley & Sons, Hoboken, New Jersey, ISBN:978-0-470-08024-5,.

Zhou, L., M.Z. Xie, M. Jia and J.R. Shi, 2011. Large eddy simulation of fuel injection and mixing process in a diesel engine. Acta Mech. Sin., 27: 519-530.

Zong, N. and V.I.G.O.R. Yang, 2006. Cryogenic fluid jets and mixing layers in transcritical and supercritical environments. Combust. Sci. Technol., 178: 193-227.

Zong, N., H. Meng, S.Y. Hsieh and V. Yang, 2004. A numerical study of cryogenic fluid injection and mixing under supercritical conditions. Phys. Fluids, 16: 4248-4261.